General and robust covalently linked graphene oxide affinity grids for high-resolution cryo-EM

Feng Wang[a], Yanxin Liu[a,1], Zanlin Yu[a,1], Sam Li[a], Shengjie Feng[b], Yifan Cheng[a,c], and David A. Agard[a,2]

[a]Department of Biochemistry and Biophysics, University of California, San Francisco, CA 94143; [b]Department of Physiology, University of California, San Francisco, CA 94158; and [c]Howard Hughes Medical Institute, University of California, San Francisco, CA 94158

Contributed by David A. Agard, July 2, 2020 (sent for review May 16, 2020; reviewed by John L. Rubinstein and Hongwei Wang)

Affinity grids have great potential to facilitate rapid preparation of even quite impure samples in single-particle cryo-electron microscopy (EM). Yet despite the promising advances of affinity grids over the past decades, no single strategy has demonstrated general utility. Here we chemically functionalize cryo-EM grids coated with mostly one or two layers of graphene oxide to facilitate affinity capture. The protein of interest is tagged using a system that rapidly forms a highly specific covalent bond to its cognate catcher linked to the grid via a polyethylene glycol (PEG) spacer. Importantly, the spacer keeps particles away from both the air–water interface and the graphene oxide surface, protecting them from potential denaturation and rendering them sufficiently flexible to avoid preferential sample orientation concerns. Furthermore, the PEG spacer successfully reduces nonspecific binding, enabling high-resolution reconstructions from a much cruder lysate sample.

cryo-EM | graphene oxide | affinity grid | single-particle reconstruction

Owing to a series of technological breakthroughs, single-particle cryo-electron microscopy (EM) is fast becoming the method of choice for determining protein structures at a near-atomic or atomic resolution (1, 2). In contrast to the rapidity of data collection and processing, sample preparation remains slow and in many cases has become rate-limiting. Cryo-EM specimens are typically prepared by depositing purified proteins onto cryo-EM grids, typically metal grids covered with continuous perforated carbon or gold film. After excess sample solution is removed by blotting, the grid is plunged into liquid ethane, vitrifying the biological sample in amorphous ice (3). Proteins of interest are thus preserved in hydrated state (4).

For challenging systems and dynamic complexes, the typical path of overexpression, biochemical-scale purification, and concentration can be problematic, either because the system cannot be overexpressed or reconstituted or because aggregation may occur. Perhaps even more significant is the disruption of protein structure and protein–protein interactions that can occur when exposed to the air–water interface (5). During formation of the thin vitreous ice films (often <50 nm) required for high-resolution imaging, the high surface area-to-volume ratio dramatically increases the probability of exposure to the potentially denaturing interface. Indeed, after vitrification, most particles are observed at the air–water interface (6) and obtaining high-resolution structures typically requires selecting only a small subset of picked particles.

A potential solution to both the sample preparation and air–water interface problems is through the use of "affinity grids" that would simultaneously concentrate the sample on the grid while restricting it from the air–water interface. Over the past decades, several affinity grid strategies for cryo-EM have been proposed, including decorating a supporting film with nickel-nitrilotriacetic acid (Ni-NTA) to capture His-tagged proteins (7–10), using 2D streptavidin crystals to capture biotin- or strep-tagged proteins (11, 12), and using specific antibodies to capture viruses (13, 14).

Yet despite these promising advances, no single strategy has proven broadly useful, owing to the inefficiency of His tags, the high scattering of thick support films, the need for specific antibodies, and other factors. Here we present an affinity grid approach that combines a small, essentially infinite affinity covalent tagging system with chemically derivatized graphene oxide (GO) support films only one to two molecules thick (Fig. 1). The self-ligating SpyCatcher/SpyTag coupling system (15) forms a covalent bond between the ~14-KDa SpyCatcher and the 12-residue SpyTag peptide, either of which can be fused to the protein of interest and the partner then coupled to the grid. The irreversible covalent bond forms within minutes (15) and is highly specific and robust, ultimately paving the way for "purification on the grid."

GO was selected as the supporting film because 1) it significantly reduces background compared with amorphous carbon (16); 2) is decorated with abundant oxygen-containing functional groups, which facilitate further chemical modification; and 3) is more straightforward to make and coat grids with than pure graphene crystals. Once a grid matrix and tagging system have been selected, the next challenge is to reduce nonspecific grid interactions and to position the sample away from the grid surface as well as the air–water interface, thereby avoiding potential sample denaturation or preferred orientation problems. For this, we choose to use a polyethylene glycol (PEG) spacer, which is known to effectively block nonspecific adsorption (17–19).

Significance

Despite the increasing efforts in developing affinity grids to facilitate sample preparation for challenging systems and dynamic complexes, they are not widely used in cryo-electron microscopy (EM) owing to concerns of limiting resolution. We show that our affinity grids extract proteins through covalent bonding with 3.3-Å reconstruction. To our knowledge, no example of small proteins (<200 KDa) has been successfully tested with other affinity grids. With encouraging results further from a mixture sample, we believe that the strategy described here is highly applicable to a broad array of challenging macromolecules and thus is a method of broad interest to the cryo-EM community. The dramatic improvement in cryo-EM sample preparation outlined here paves the way to "purification on the grid."

Author contributions: F.W., Y.C., and D.A.A. designed research; F.W., Y.L., Z.Y., S.L., and S.F. performed research; F.W., Y.L., Z.Y., S.L., and S.F. analyzed data; F.W., Y.L., Z.Y., S.L., and S.F. wrote the paper with input from Y.C.; and Y.C. and D.A.A. supervised the project.

Reviewers: J.L.R., The Hospital for Sick Children Research Institute; and H.W., Tsinghua University.

F.W., Y.C., and D.A.A. are authors on the patent application entitled "Graphene oxide affinity sample grids for cryo-em" (publication number WO2020041202A1).

[1]Y.L. and Z.Y. contributed equally to this work.

[2]To whom correspondence may be addressed. Email: agard@msg.ucsf.edu.

This article contains supporting information online at https://www.pnas.org/lookup/suppl/doi:10.1073/pnas.2009707117/-/DCSupplemental.

First published September 10, 2020.

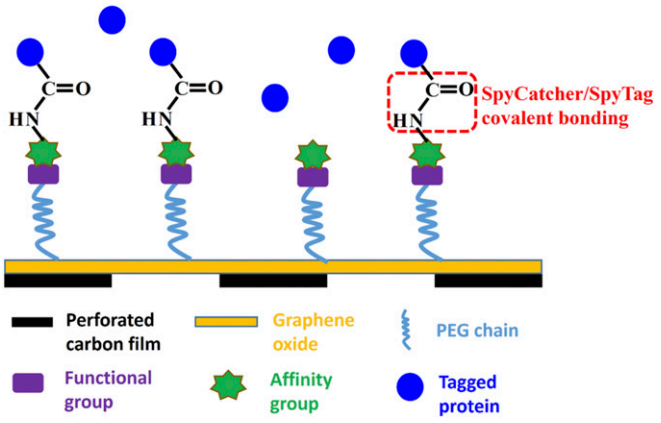

Fig. 1. Schematic illustration of the affinity grid assembly.

Results

Assembly of GO Affinity Grids. To optimize the substrate for coverage and chemical reactivity, we synthesized GO using a modified Hummer's method (20), rather than using commercially available preparations that have smaller sheets and greater variation in oxygen content. Elemental analysis from X-ray photoelectron spectroscopy (XPS) gave a C/O ratio of ~2, indicating a relatively high level of oxidation (*SI Appendix*, Fig. S1). To reproducibly make EM grids with a uniform GO coverage, we established a simple, robust procedure involving spreading GO films at the air–water interface and lowering them onto submerged grids (21), derived from a previously described method (22). We estimated GO coverage of >90% of grid surface, with ~40% monolayer, 40% bilayer, and <20% with three or more layers. In agreement with our previous experience (21), we did not notice any negative impact of the GO on contrast in the cryo-EM image even with very small particles (~150 kDa). As shown in Fig. 2*A*, a typical TEM image at lower magnification indicates full coverage of GO over the grid square. Monolayer GO (Fig. 2*B*) and double-layer GO (*SI Appendix*, Fig. S2) over carbon holes can be observed by selected area electron diffraction.

Considering that carboxyl groups mainly decorate on the edges of GO sheets, we decided to primarily use the epoxide groups that cover the bulk of planar area (23) for functionalization. As illustrated previously (24), epoxide groups are efficiently functionalized via nucleophilic reaction with primary amines (*SI Appendix*, Fig. S3) under nonaqueous conditions. In addition, under these conditions, the much smaller number of carboxyl groups will also react with the amine to form amide bonds. To maximize versatility, we first coupled an amino-PEG-alkyne linker to the grid and then coupled a target-specific reactive azide-PEG spacer in a second step using Cu-free click chemistry (25). Because the GO-PEG-alkyne grids are quite stable, this allows the use of a wide range of coupling chemistries/reactive groups to link the tag catcher to the grid. In the example reported here, we used an azide-PEG-maleimide to couple to a cysteine on the SpyTag or SpyCatcher to preformed PEG-alkyne grids. Alternatively, one could use an azide-PEG-*N*-hydroxy succinimide to couple to primary amines or directly couple other azide-containing tags. The presence of the PEG segment helps passivate the grid surface, renders it sufficiently hydrophilic for good vitrification, spaces the target away from the surface, and increases the flexibility to minimize potential issues with preferential orientation. We note that proteins often aggregated or disassembled on the functionalized copper grids. We speculate that copper was involved in the Cu-free reaction and released substances that complicated the sample preparation. This problem was avoided by using gold holey carbon grids throughout our experiments, although we could just as easily have used gold foil on gold grids.

Evaluation of GO Affinity Grids as a Broadly Useful Strategy. After coupling of the SpyTag or SpyCatcher to the maleimide grids, incubation with a cognate-tagged protein of interest efficiently forms a stable attachment in a matter of minutes. Although we have used this procedure attaching either SpyTag or SpyCatcher to the grid, in the example here we incubated a SpyTag grid with a dilute solution (270 nM) of the dimeric human mitochondrial Hsp90 molecular chaperone (TRAP1, ~150 kDa) fused to either SpyTag (control) or SpyCatcher (cognate sample; total molecular weight ~165 KDa). The grids were extensively washed to remove unbound or loosely adsorbed proteins. As demonstrated in Fig. 3*A*, in the noncognate control sample, few TRAP1 molecules are visible. In contrast, applying TRAP1-SpyCatcher to the same SpyTag affinity grids (Fig. 3*B*) resulted in a satisfactory particle density (~250 particles per micrograph) and was suitable for high-resolution studies. This clearly demonstrates successful and specific affinity capture on the grid with the SpyCatcher/SpyTag system. Obtaining a similar particle density on a regular grid (Quantifoil holey carbon gold grid, 300 mesh) required a concentration of ~2 μM, indicating the ability of the affinity grid to specifically concentrate the protein of interest. High-resolution features of TRAP1 are clearly visible in the 2D class averages (Fig. 3*C*) and suggest that the data collected are of high quality with a minimal impact on contrast from grid modification.

In the current study, we used the human mitochondrial Hsp90 (TRAP1) as a test sample. This sample is much smaller (~150 kDa) than the samples typically used for testing grid technologies, such as proteasomes or ribosomes, making it a stringent test of grid background, contrast, and achievable ice thickness. It also turns out to be particularly sensitive to partial denaturation at the air–water interface (see below). Each TRAP1 protomer within the dimer consists of three individual domains: the N-terminal domain (NTD), middle domain (MD), and C-terminal domain (CTD). Together, these domains go through a complex ATP binding and hydrolysis cycle (26) that plays a key role in regulating mitochondrial protein homeostasis and function. Although the crystal structure of TRAP1 from zebrafish had been determined previously (27), human TRAP1 has proven to be a significant challenge for both X-ray crystallography (producing only poorly diffracting crystals) and cryo-EM. Despite the ability to collect a large, high-quality dataset, previous attempts at solving the human TRAP1 cryo-EM structure using standard Quantifoil grids mainly

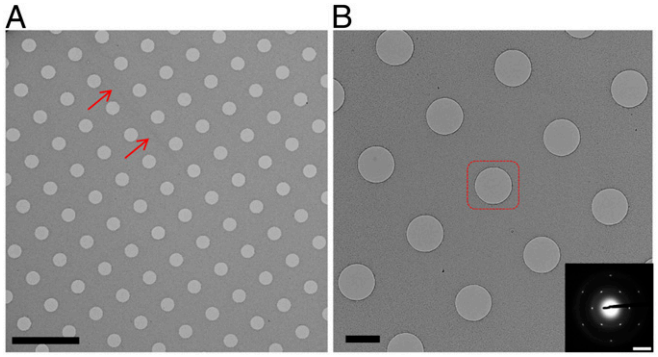

Fig. 2. GO deposition onto EM grids. (*A*) TEM image at 2,500× magnification showing full coverage of GO on the grid. Two arrows point to a long wrinkle, which may be due to GO overlapping. (Scale bar: 5 μm.) (*B*) TEM image at 5,000× magnification showing GO coating of single layer. (Scale bar: 1 μm.) (*Inset*) Selected area electron diffraction taken from the center hole marked by the dashed square. (Scale bar: 5 nm^{-1}.)

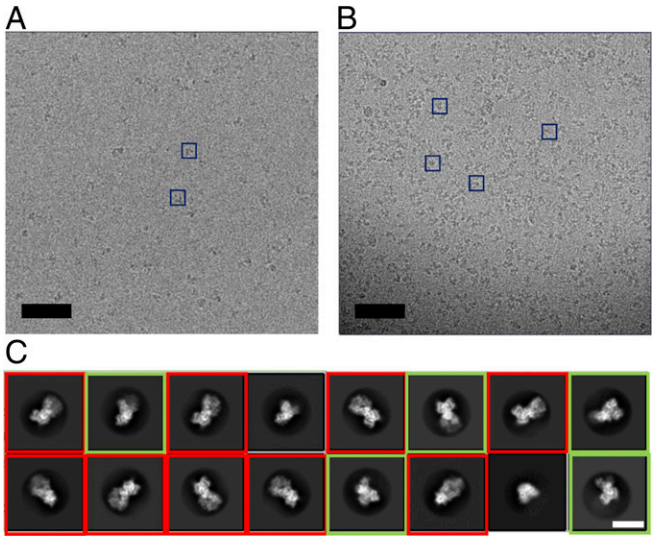

Fig. 3. Affinity testing using TRAP1 as a test sample on the SpyTag-PEG (5,000 Da)-GO grid. (*A*) Noncognate tag control grid. A cropped cryo-EM control micrograph of human mitochondrial Hsp90 (TRAP1)-SpyTag applied to a SpyTag-PEG (5,000 Da)-GO affinity grid obtained with an FEI Talos Arctica transmission electron microscope with a Gatan K3 camera. Representative protein particles are boxed by blue squares. (Scale bar: 50 nm.) (*B*) Cropped cryo-EM micrograph of TRAP1-SpyCatcher applied to the same type of SpyTag-PEG (5,000 Da)-GO affinity grid used in *A*. Representative protein particles are boxed by blue squares. The image was taken on an FEI Titan Krios transmission electron microscope with a Gatan K2 camera. (Scale bar: 50 nm.) (*C*) Selected 2D class averages of nucleotide-bound TRAP1-SpyCatcher using affinity grids as described in *B*. Full-length classes are boxed by red squares, and classes with missing CTDs are boxed with green squares. (Scale bar: 10 nm.)

produced a structure in which only the TRAP1 NTD and MD from each protomer were resolved (4.1 Å; Fig. 4*A*). Notably, this structure differs from a crystal structure of TRAP1 in which the CTDs are proteolyzed and crystallized after closure (27). Only a minor population of particles representing full-length TRAP1 could be classified in 3D (class II in *SI Appendix*, Fig. S4*B*), resulting in a medium-resolution reconstruction even when starting with a large dataset (4.3 Å; Fig. 4*B*). Both the classes with a disrupted CTD and the full-length classes are indicated in the 2D class averages from this dataset (*SI Appendix*, Fig. S5). The dimerization interface between the NTDs of each protomer is preserved in the dominant structure (Fig. 4*A*), which only happens when starting with full-length protein. Thus, the disruption of the CTD dimerization interface most likely occurs on grid preparation, presumably due mainly to the interaction with the air–water interface, resulting in a disordered CTD that is invisible in our reconstructions.

Fortunately, our GO-based affinity grids solve this problem, and full-length particles are readily visible in the raw micrographs (Fig. 3*B*) as well as in the 2D class averages (Fig. 3*C*). We hypothesize that the preservation of the TRAP1 CTD dimerization interface is due to the affinity tags keeping the protein away from the postblotting air–water interface, where air exposure would be expected to be most severe. As demonstrated by tomography, the PEG spacer keeps the protein away from both the air–water interface and the GO surface, thereby avoiding potentially unfavorable interactions with both surfaces (*SI Appendix*, Fig. S6 and Movie S1). It is interesting to note that the observed distance between the sample and the GO surface (11.4 nm) is intermediate between the distance expected for a fully extended PEG (5,000 Da) spacer (~31.8 nm) and a PEG (5,000 Da) spacer behaving as a random chain (~4.7 nm). Although the TRAP1 dimer state missing the CTD density was still present in our affinity grid dataset (reconstructed to 3.1-Å resolution; Fig. 4*C*), the fraction of full-length TRAP1 population was improved from 3.0% (with three rounds of 3D classification required to identify the full-length structure) to 12.3% (after only one round of 3D classification) (*SI Appendix*, Figs. S4 and S7). We have shown previously that the simultaneous dimerization of NTDs and CTDs in the full-length TRAP1 results in a highly strained "closed" state (27). TRAP1 CTD opening releases such strain. Presumably, the air–water interface biases the equilibrium toward the TRAP1 CTD open state, as it minimizes the energetic cost of exposing the hydrophobic inter-CTD interface. By keeping the protein away from the air–water interface, the affinity grid helps protect the CTDs, increasing the population of full-length proteins. However, other factors, such as the internal strain mentioned above, may still be contributing to CTD opening and disruption. Using the affinity grids, we were able to solve the full-length TRAP1 structure at 3.3-Å resolution (Fig. 4*D*). This structure closely resembles the crystal structure of zebrafish TRAP1 and exhibits the same pronounced asymmetry (27), proving that this distinctive conformation is conserved across species and that it is not a consequence of crystallization.

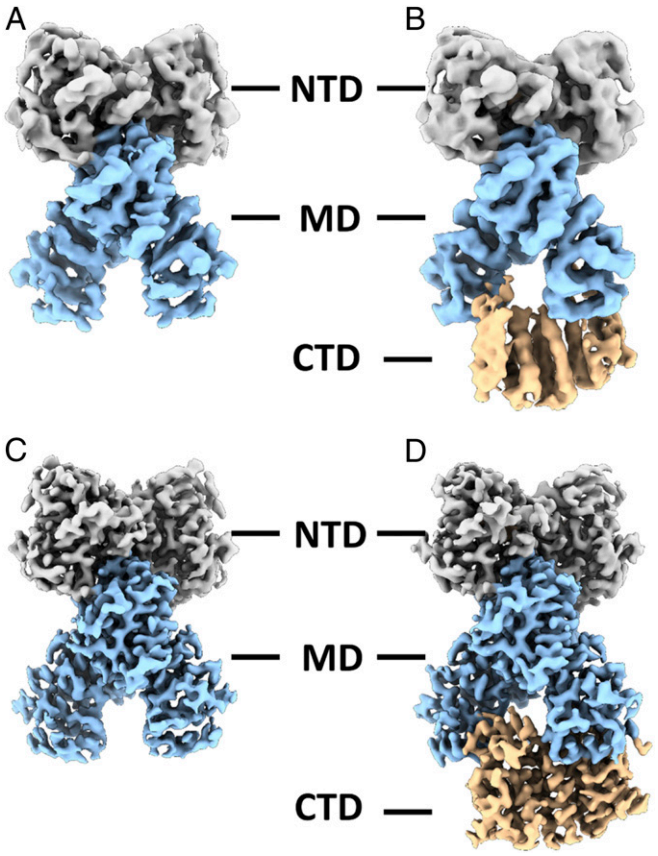

Fig. 4. 3D density maps of human TRAP1-SpyCatcher structures determined using both regular Quantifoil grids and GO-based affinity grids. (*A*) TRAP1-SpyCatcher structure (4.1 Å) with a disrupted and invisible CTD obtained from the dominant class using regular Quantifoil grids. (*B*) Full-length TRAP1-SpyCatcher structure (4.3 Å) obtained from a minor class of particles using regular Quantifoil grids. (*C*) Structure of TRAP1-SpyCatcher with a disrupted invisible CTD at 3.1-Å resolution using a SpyTag-PEG (5,000 Da)-GO affinity grid. (*D*) Full-length structure of TRAP1-SpyCatcher at 3.3-Å resolution using a SpyTag-PEG (5,000 Da)-GO affinity grid. The SpyCatcher was not visible in all cases. The TRAP1 NTD, MD, and CTD are colored gray, blue, and yellow, respectively.

Having datasets for the same sample using both conventional grids and the affinity grids reveals clear differences in orientation bias. From the 2D class averages, side views are quite rare with conventional grids but prevalent with the affinity grids. The angular distributions for each final reconstruction are shown in *SI Appendix*, Fig. S8.

Although it was not an issue here, there is the possibility that with other systems, tethering via the affinity tag may problematically bias particle orientation. Possible remedies might include 1) increasing the length of the PEG linker, 2) changing where the SpyCatcher is connected to the PEG linker, 3) increasing the length of the linker between the protein of interest and the complimentary tag, or 4) changing the site on the protein to be tagged. These strategies are not mutually exclusive and could be used synergistically to optimize the particle orientation on the grid.

To further evaluate the SpyCatcher/SpyTag affinity grid, we also tested the reverse configuration, immobilizing SpyCatcher on the grid and then applying TRAP1-SpyTag. We also explored two different PEG chain lengths (molecular weight 600 Da with a fully extended length of 3.8 nm and molecular weight 5,000 Da with an extended length of 31.8 nm) (28) in the azide-PEG-maleimide spacer. While we did not pursue full reconstructions in these cases, there were no apparent differences in either particle density or 2D class average quality (*SI Appendix*, Figs. S9–S17). Moreover, we further tested selectivity of the SpyCatcher affinity grid using a completely different sample, apoferritin, fused with SpyTag to demonstrate generality (*SI Appendix*, Figs. S18–S20).

As another example, we tested tagging the scaffold protein used in forming nanodiscs to the grid by fusing SpyTag to the scaffold protein. Reconstituted nanodiscs were then incubated with SpyCatcher grids (*SI Appendix*, Figs. S21 and S22). This extends the utility of our affinity grid to membrane proteins. Particularly useful is the perpendicular orientation to the grid of many of the nanodiscs, providing an optimal orientation for reconstruction of an included membrane protein.

GO Affinity Grids Can Selectively Enrich for the Sample Out of a Crude Lysate. Ultimately, our desire is to reduce nonspecific background to the extent that target molecules can be purified on the grid directly from native sources. Here we established a controlled test, mimicking an actual cell lysate by premixing apoferritin-SpyTag with crude rabbit reticulocyte lysate at a 1:9 ratio (apoferritin-SpyTag 0.04 mg/mL [~69 nM, molecular weight 580 kDa] and rabbit reticulocyte lysate 0.36 mg/mL). To further passivate the grid surface to reduce nonspecific background, hydroxyl-capped PEG was introduced in the functionalization step at a 9:1 ratio of hydroxyl PEG azide:maleimide PEG-azide. Use of the hydroxyl-PEG successfully reduced nonspecific binding. With apoferritin particles distinctly visible on the raw micrograph (Fig. 5*A*), a structure with a resolution of 2.65 Å was obtained (Fig. 5*B*). The first round of 2D classification is shown in *SI Appendix*, Fig. S23.

Discussion and Conclusion

In summary, our GO-based affinity grids provide selective enrichment of a tagged sample on the grid. As demonstrated by the exemplary protein TRAP1, image contrast and particle orientation were not negatively impacted by tethering to GO via the PEG-SpyCatcher/SpyTag. This allows ready reconstruction of even small (<200 kDa) particles at high resolution, which, to our knowledge, has not been demonstrated with any of the other types of affinity grids reported to date. Perhaps even more importantly, the ability of our affinity grids to protect delicate samples from potential partial denaturation/aggregation at the air–water interface may prove to be an enabling technology. Here this allowed us to determine the full-length structure of human TRAP1 at atomic resolution, paving the way for future structure-based drug discovery experiments. Furthermore, the encouraging outcomes from testing on controlled lysate mixtures

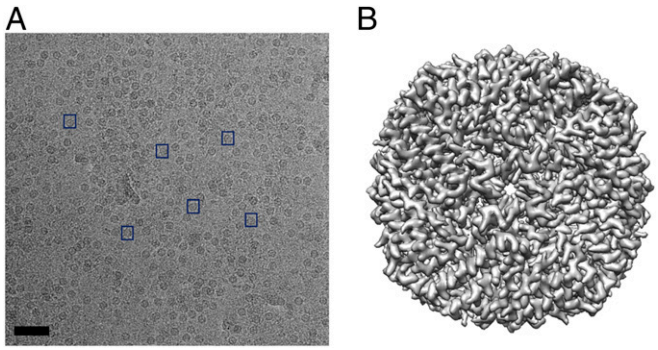

Fig. 5. Affinity testing using Apoferritin-SpyTag/rabbit reticulocyte mixture as a test sample on the SpyCatcher/hydroxyl-PEG (5,000 Da)-GO grid. (*A*) Cryo-EM micrograph of apoferritin-SpyTag bound to a SpyCatcher/hydroxyl-PEG (5,000 Da)-GO affinity grid. Representative protein particles are boxed by blue squares. The image was taken on an FEI Tecnai Polara cryo transmission electron microscope with a Gatan K2 camera. (Scale bar: 50 nm.) (*B*) Reconstruction of apoferritin-SpyTag at a resolution of 2.65 Å.

suggest that our affinity grids have great potential to achieve "purification on the grid." Further work on other complex mixture systems is currently underway.

It is noteworthy that our grid modification strategy readily allows the use of other affinity tagging pairs beyond the SpyCatcher/SpyTag system used here. For example, SnapTag or HaloTag ligands could be coupled to the grids, allowing the purification of SnapTagged or HaloTagged proteins often favored by cell biologists for the ability to incorporate small-molecule fluorophores for in vivo light microscopy (29). DNA, RNA, nanobodies, etc., can also be readily incorporated, extending the practical applications to a much broader range of biological problems. Alternatively, for use with pure proteins/complexes, the grid surface or the PEG terminus can be modified to display primary or secondary amines or other chemical chemotypes. For example, we have found that amino-GO or amino-PEG-GO grids wet better, promote protein adsorption, and improve orientation distribution compared with bare GO grids (30).

Materials and Methods

GO Synthesis. GO was synthesized via the modified route developed by Marcano et al. (20). Into the mixture of concentrated sulfuric acid (120 mL; Ward's Science, 470302-872) and phosphoric acid (13 mL; Sigma-Aldrich, 345245), graphite flakes (1 g; Sigma-Aldrich, 332461) were added. Potassium permanganate (6 g; Sigma-Aldrich, 223468) was slowly added, after which the mixture was placed in a water bath at 45 °C and stirred overnight. The reaction mixture was then moved into an ice bath and deionized (DI) water (100 mL) was poured in, followed by the addition of 30% H_2O_2 (1.5 mL; Sigma-Aldrich, 216763). The mixture was allowed to sit for 2 h and was then centrifuged at 5,000 rpm for 20 min. The solid material at the bottom was retrieved and washed extensively with DI water by centrifugation until the pH reached 5. Finally, the remaining viscous material was collected and stirred overnight to make a GO stock solution in water. After drying at 80 °C, XPS measurements were performed on GO flakes with a PerkinElmer PHI 5600 X-ray photoelectron spectrometer.

GO Deposition onto EM Grids. To coat GO sheets onto EM grids, we revised the Langmuir–Blodgett assembly method as described by Cote et al. (22) and also reported in our previous work (21). The GO water stock solution was diluted with methanol/water (5:1, v:v) to a concentration of 0.1 mg/mL. Mild stirring for 30 min rather than sonication was used to avoid destruction of GO sheets, producing a GO working solution. An epoxy-coated stainless steel mesh (McMaster–Carr) stand was placed at the bottom of a glass Petri dish (60 mm diameter, 15 mm tall), and DI water was filled to the top. EM grids (Au Quantifoil, 300 mesh) were used as received and placed on the mesh with the carbon side facing up. Then a total volume of 230 μL of GO working solution was spread dropwise onto the water surface at different spots at a speed of 50 μL/min using a syringe. Once the water was drained, the

GO-coated grids were dried at room temperature overnight for use. Coverage of GO was examined on an FEI Tecnai 20 transmission electron microscope (Thermo Fisher Scientific) with an acceleration voltage of 200 kV.

Surface Modification of GO-Coated EM Grids. In a 1.5-mL centrifuge microtube, one GO-coated EM grid (GO grids) was submerged in 20 μL of dibenzocyclooctyne-PEG-amine (DBCO-PEG4-amine; Click Chemistry Tools, A103P) solution in dimethyl sulfoxide (DMSO) at a concentration of 10 mM and shaken at room temperature overnight. Following that, the DBCO functionalized grid was washed three times with DMSO and DI water respectively, and then submerged in 20 μL of azide-PEG-maleimide (molecular weight 600 Da; Nanocs, PG2-AZML-600 or molecular weight 5,000 Da; Nanocs, PG2-AZML-5k) solution in DI water at a concentration of 4 mM. Alternatively, hydroxyl-capped PEG was introduced at this step to reduce nonspecific binding. Azide-PEG-maleimide (molecular weight 5,000 Da; Nanocs, PG2-AZML-5k) was mixed with azide-PEG-hydroxyl (molecular weight 5,000 Da; Nanocs, PG2-AZOH-5k) in DI water at a ratio of 1:9 to form a solution with a total PEG concentration of 4 mM. The reaction was shaken at room for 6 h, and the grid was washed three times with DI water and ethanol, respectively. The as-made maleimide grid or maleimide/hydroxyl grid was then dried in ambient air for 30 min and stored at −20 °C for future use.

Details of protein purification, assembly and vitrification using affinity grids, cryo-EM data acquisition, image processing, and tomography analysis are provided in *SI Appendix, Materials and Methods*. The washing process during grid freezing is illustrated in Movie S2.

Data Availability. Maps and coordinates have been deposited in the Electron Microscopy Data Bank (EMD accession codes 22174–22177) and the Protein Data Bank, (PDB ID code 6XG6).

ACKNOWLEDGMENTS. We thank Eugene Palovcak for helpful discussions; Michael Braunfeld, Alex Myasnikov, David Bulkley for help and running the University of California San Francisco Advanced Cryo-Electron Microscopy Facility; and Matt Harrington for high performance computing (HPC) support. D.A.A. is funded by a University of California San Francisco Program for Breakthrough Biomedical Research technology development grant and NIH grants R35 GM118099, U54 CA209891, U01 MH115747, and U19 AI135990. Y.C. is supported by NIH grants R01 GM098672, P50 GM082250, and P01 GM11126. Y.C. is supported by the Howard Hughes Medical Institute, and the facility has received NIH instrumentation grants S10 OD020054 and S10 OD021741. Y.L. was supported by a Howard Hughes Medical Institute–Helen Hay Whitney Foundation Postdoctoral Fellowship, an American Heart Association Postdoctoral Fellowship (18POST33990362), and the Program for Breakthrough Biomedical Research, which is partially funded by the Sandler Foundation.

1. Y. Cheng, Single-particle cryo-EM at crystallographic resolution. *Cell* **161**, 450–457 (2015).
2. E. Nogales, The development of cryo-EM into a mainstream structural biology technique. *Nat. Methods* **13**, 24–27 (2016).
3. J. P. Renaud *et al*., Cryo-EM in drug discovery: Achievements, limitations and prospects. *Nat. Rev. Drug Discov.* **17**, 471–492 (2018).
4. K. A. Taylor, R. M. Glaeser, Electron diffraction of frozen, hydrated protein crystals. *Science* **186**, 1036–1037 (1974).
5. E. D'Imprima *et al*., Protein denaturation at the air-water interface and how to prevent it. *eLife* **8**, e42747 (2019).
6. A. J. Noble *et al*., Routine single particle CryoEM sample and grid characterization by tomography. *eLife* **7**, e34257 (2018).
7. C. J. Benjamin *et al*., Selective capture of histidine-tagged proteins from cell lysates using TEM grids modified with NTA-graphene oxide. *Sci. Rep.* **6**, 32500 (2016).
8. M. C. Llaguno *et al*., Chemically functionalized carbon films for single molecule imaging. *J. Struct. Biol.* **185**, 405–417 (2014).
9. D. F. Kelly, D. Dukovski, T. Walz, Monolayer purification: A rapid method for isolating protein complexes for single-particle electron microscopy. *Proc. Natl. Acad. Sci. U.S.A.* **105**, 4703–4708 (2008).
10. N. Liu *et al*., Bioactive functionalized monolayer graphene for high-resolution cryo-electron microscopy. *J. Am. Chem. Soc.* **141**, 4016–4025 (2019).
11. B. G. Han *et al*., Electron microscopy of biotinylated protein complexes bound to streptavidin monolayer crystals. *J. Struct. Biol.* **180**, 249–253 (2012).
12. I. Lahiri *et al*., 3.1 Å structure of yeast RNA polymerase II elongation complex stalled at a cyclobutane pyrimidine dimer lesion solved using streptavidin affinity grids. *J. Struct. Biol.* **207**, 270–278 (2019).
13. D. F. Kelly, D. Dukovski, T. Walz, Strategy for the use of affinity grids to prepare non-His-tagged macromolecular complexes for single-particle electron microscopy. *J. Mol. Biol.* **400**, 675–681 (2010).
14. G. Yu *et al*., Single-step antibody-based affinity cryo-electron microscopy for imaging and structural analysis of macromolecular assemblies. *J. Struct. Biol.* **187**, 1–9 (2014).
15. B. Zakeri *et al*., Peptide tag forming a rapid covalent bond to a protein, through engineering a bacterial adhesin. *Proc. Natl. Acad. Sci. U.S.A.* **109**, E690–E697 (2012).
16. R. S. Pantelic, J. C. Meyer, U. Kaiser, W. Baumeister, J. M. Plitzko, Graphene oxide: A substrate for optimizing preparations of frozen-hydrated samples. *J. Struct. Biol.* **170**, 152–156 (2010).
17. K. L. Prime, G. M. Whitesides, Adsorption of proteins onto surfaces containing end-attached oligo(ethylene oxide): A model system using self-assembled monolayers. *J. Am. Chem. Soc.* **115**, 10714–10721 (1993).
18. S. I. Jeon, J. D. Andrade, Protein-surface interactions in the presence of polyethylene oxide. *J. Colloid Interface Sci.* **142**, 149–158 (1991).
19. C. J. Benjamin *et al*., Nonfouling NTA-PEG-based TEM grid coatings for selective capture of histidine-tagged protein targets from cell lysates. *Langmuir* **32**, 551–559 (2016).
20. D. C. Marcano *et al*., Improved synthesis of graphene oxide. *ACS Nano* **4**, 4806–4814 (2010).
21. E. Palovcak *et al*., A simple and robust procedure for preparing graphene-oxide cryo-EM grids. *J. Struct. Biol.* **204**, 80–84 (2018).
22. L. J. Cote, F. Kim, J. Huang, Langmuir-Blodgett assembly of graphite oxide single layers. *J. Am. Chem. Soc.* **131**, 1043–1049 (2009).
23. D. R. Dreyer, S. Park, C. W. Bielawski, R. S. Ruoff, The chemistry of graphene oxide. *Chem. Soc. Rev.* **39**, 228–240 (2010).
24. D. Luo *et al*., Nanofluid of graphene-based amphiphilic Janus nanosheets for tertiary or enhanced oil recovery: High performance at low concentration. *Proc. Natl. Acad. Sci. U.S.A.* **113**, 7711–7716 (2016).
25. J. M. Baskin *et al*., Copper-free click chemistry for dynamic in vivo imaging. *Proc. Natl. Acad. Sci. U.S.A.* **104**, 16793–16797 (2007).
26. K. A. Krukenberg, T. O. Street, L. A. Lavery, D. A. Agard, Conformational dynamics of the molecular chaperone Hsp90. *Q. Rev. Biophys.* **44**, 229–255 (2011).
27. L. A. Lavery *et al*., Structural asymmetry in the closed state of mitochondrial Hsp90 (TRAP1) supports a two-step ATP hydrolysis mechanism. *Mol. Cell* **53**, 330–343 (2014).
28. F. Oesterhelt, M. Rief, H. E. Gaub, Single molecule force spectroscopy by AFM indicates helical structure of poly(ethylene-glycol) in water. *New J. Phys.* **1**, 6 (1999).
29. G. V. Los *et al*., HaloTag: A novel protein labeling technology for cell imaging and protein analysis. *ACS Chem. Biol.* **3**, 373–382 (2008).
30. F. Wang *et al*., Amino and PEG-amino graphene oxide grids enrich and protect samples for high-resolution single particle cryo-electron microscopy. *J. Struct. Biol.* **209**, 107437 (2020).